Sensors & Actuators: B. Chemical 320 (2020) 128292

Contents lists available at ScienceDirect

Sensors and Actuators B: Chemical

journal homepage: www.elsevier.com/locate/snb

High-performance acetone gas sensor based on Ru-doped SnO_2 nanofibers

Xueying Kou, Fanqi Meng, Ke Chen, Tianshuang Wang, Peng Sun*, Fangmeng Liu, Xu Yan, Yanfeng Sun, Fengmin Liu, Kengo Shimanoe, Geyu Lu*

State Key Laboratory on Integrated Optoelectronics, Jilin Province Key Laboratory on Advanced Gas Sensors, College of Electronic Science and Engineering, Jilin University, 2699 Qianjin Street, Changchun 130012, People's Republic of China

ARTICLE INFO

Keywords:
Ru-doped SnO_2 nanofibers
Electrospinning
Acetone
Gas sensor

ABSTRACT

We report the Ru doping effect on the gas-sensing properties of SnO_2 nanofibers for acetone detection in this paper. For this purpose, pure and 1, 2, 3 mol% Ru-doped SnO_2 nanofibers were prepared through electrospinning technique combined with calcination treatment. The fibrous microstructure of these nanofibers were maintained and the grain size of the SnO_2 nanoparticals were decreased from 9.2 nm (pure) to 5.1 nm (3% Ru-doped) after Ru doping. In order to confirm that Ru doping is an effective way to improve the gas sensing properties of the SnO_2-based gas sensor, the gas sensing properties of the sensors based on pure and Ru doped SnO_2 nanofibers were investigated systematically. The results showed that the response to 100 ppm acetone of 2 mol% Ru-doped SnO_2 nanofibers was 118.8, which was 12 times higher than that of pure SnO_2 nanofibers. In the end, the role of Ru in the gas sensing mechanism of SnO_2 nanofibers was analyzed according to the results of the X-ray photoelectron spectroscopy (XPS) and Ultraviolet photoelectron spectroscopy (UPS).

1. Introduction

As one of the widely researchful chemiresistive sensors, the one adopting semiconducting metal oxides (SMOs) as sensing materials, has become the focus due to its low cost, high stability, simple operation principle and easy fabrication [1,2]. Up to now, many promising SMOs sensing materials, such as SnO_2 [3,4], In_2O_3 [5,6], ZnO [7,8], a-Fe_2O_3 [9,10], WO_3 [11,12], NiO [13,14] and so on, have been continuously reported for the use of detecting poisonous and flammable gases. As for the effective methods of improving gas sensing properties of SMOs sensing materials, it is particularly important to design the reasonable morphology and structure of the sensing material and adopt appropriate surface modification method. As is known to all, surface morphology and structure of the SMOs have a great influence on gas sensing properties due to the surface of the sensing materials providing the site of the interaction between gas molecules and the surface chemisorbed oxygen species. Up to now, a variety of morphologies and structures of SMOs have been synthesized through various methods such as nanoparticles [15,16], nanorods [17,18], nanosheets [19,20], nanospheres [21,22] and nanoflowers [23,24] and so on. Besides these, nanofibers have been confirmed of great potential in the application of gas sensing materials owing to their high electron mobility, large length to diameter ratio, high crystalline and uniformity [25–27]. Many sensing materials of nanofibous structure have been widely reported. Lee et al. synthesized pure and Fe-doped In_2O_3 nanofibers and demonstrated that Fe-doped could change the gas selectivity [28]. Yang et al.'s work proved that SnO_2/ZnO 1D fibrous hierarchical structure exhibited superior gas sensing response toward ethanol gas [29]. Kim et al. provided an evidence of enhanced CO and NO_2 sensing properties, using SnO_2–Cu_2O core–shell nanofibers [30]. Although morphology and structure have great influence on the gas sensing properties of nanomaterials, surface modification on the gas sensing materials also played a crucial role. A variety of modification methods have been applied to gas sensing materials. Such as aliovalent doping [31,32], two nanomaterial composite [33,34], noble metal loading [35,36] and so on. The above modification methods could improve the sensitivity and selectivity of gas sensing materials by adjusting the electron depletion layer on the surface of materials, constructing potential barriers, adjusting the carrier concentration of materials, changing the distribution of oxygen components on the surface and introducing catalysts [37,38].

In this work, pure and 1–3 mol% Ru-doped SnO_2 nanofibers were synthesized through an electrospinning process with subsequent calcination method to investigate the variation of gas sensing properties after doping. In this process, we determined the optimal Ru doping amount and investigated the effect of Ru^{4+} doping on the gas sensing properties of SnO_2 nanofibers. The results showed, the sensors based on Ru-doped SnO_2 nanofibers exhibited improved gas sensing properties to all tested gases. Notablely, the response of the 2 mol% Ru-doped SnO_2

* Corresponding authors.
E-mail addresses: pengsun@jlu.edu.cn (P. Sun), lugy@jlu.edu.cn (G. Lu).

https://doi.org/10.1016/j.snb.2020.128292
Received 24 January 2020; Received in revised form 29 April 2020; Accepted 11 May 2020
Available online 17 May 2020

nanofifibers to 100 ppm acetone at 200 °C was 118.8, which was 12 times higher than that of pure SnO_2 nanofibers. In the end, the possible reasons for the improvement of gas sensing properties of Ru-doped SnO_2 nanofibers were analyzed and discussed with respect to the change of the electron concentration and distribution of oxygen component caused by the incorporation of Ru^{4+} into SnO_2 nanocrystals.

2. Experimental section

2.1. Synthesis of pure and Ru-doped SnO_2 nanofibers

Pure and Ru-doped SnO_2 nanofibers with various doping amount of 1, 2 and 3 mol% were prepared by electrospinning combining with calcination treatment. As similar as our previous work [38], 5 mL DMF and 5 mL ethanol were used as a solvent to dissolve 2 mmol $SnCl_2{\cdot}2H_2O$ and a certain dose of $RuCl_3{\cdot}3H_2O$ (0.02 mmol for 1 mol%; 0.04 mmol for 2 mol%; 0.06 mmol for 3 mol%) by magnetic stirring at room temperature. Then, we put 1 g PVP into above mixture solution with continuing magnetic stir for 5 h. After above process, we got a transparent and clear precursor, which was used to electrospinning. As for the process of electrospinning, the precursor was moved into a syringe which connecting with a spinneret. The parameters of electrospinning is as follows: the voltage was 14 ± 0.5 kV and the distance between the positiv1e pole (needle) and the negative pole (collector) was 12 cm. The injection speed of the precursor was fixed at 0.3 mL/h by a peristaltic pump. The PVP/$SnCl_2$ or PVP/$SnCl_2$/$RuCl_3$ composite nanofibers mats were obtained after the electrospinning process. In the end, the four obtained samples were calcined at 500 °C for 2 h in a muffle furnace with air atmosphere to remove organic polymer components compeletly.

2.2. Characterization

The phase structures of the four samples were analyzed by X-ray diffraction (XRD) through Rigaku TTRIII X-ray diffractometer with Cu Kα radiation at a wavelength of 1.5406 Å at 40 kV and 200 mA. The external microstructures were observed by field-emission scanning electron microscopy (FESEM) (JEOL JSM-7500F, operated at an accelerating voltage of 5 kV). Transmission electron microscopy (TEM) and high-resolution TEM (HRTEM) images were obtained on a JEM-2200FS (JEOL) transmission electron microscope with an operating voltage of 200 kV to further observe the microstructures of the samples. The X-ray photoelectron spectroscopy (XPS) measurements were carried out using an ESCALAB 250 X-ray photoelectron spectrometer with an X-ray source (Al Kα hv = 1486.6 eV) and the ultroviolet photoelectron spectrometer (UPS) measurements were also collected from it with an ultraviolet source.

2.3. Fabrication and measurement of gas sensor

Fig. 1 shows the structure diagram of the fabricated gas sensor. The sensor consists of a base and a planar electrode substrate, whose characterization was described in our previous work [38]. The size of the electrode substrate are 1.5 mm × 1.5 mm and the thickness is 0.2 mm. Fig. 1(a) and (b) are the front and back of the electrode substrate. The electrode substrate adopts alumina ceramic plate as the main body, which was coated with two "L" shape gold electrodes on the front side (electrode widths = 0.3 mm; separation = 0.15 mm) and RuO_2 heating layer on the back side. The as-prepared sensing materials (pure, 1, 2, 3 mol% Ru-doped SnO_2 nanofibers) were mixed with deionized water to form a homogeneous viscous paste, respectively. Then the pastes were coated onto the front surface of planar electrode substrate. The operating temperatures of the sensors were adjusted by changing the working current or voltage of the electrode substrate. The heating current or voltage corresponding to the operating temperature value were measured by an FLIR temperature sensor (T250, FLIR

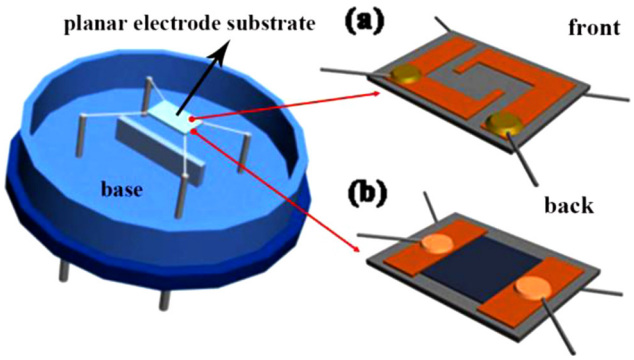

Fig. 1. Schematic diagram of the gas sensor and the (a) front (b) back of the planar electrode substrate.

Systems Inc., USA). Subsequently, the resulting sensing device was calcined at 400 °C for 2 h to enhance the stability of the sensing materials. The gas sensing properties of sensors based on pure and Ru-doped SnO_2 nanofibers were investigated by a static gas sensing characterization system under laboratory conditions (30% relative humidity, 20 °C), which were shown in Fig. 2. The static gas sensing characterization system consists of a constant current source, a high precision digital multimeter, a computer and two test chambers. At first, the sensor was stayed in chamber 1, which was full of fresh air and its resistance in air maintained a certain value, noted as R_a. Then, a certain amount of target test gas was injected into chamber 2 using a microsyringe which was washed by fresh air. After that, the sensor was put into the chamber 2 quickly to react with the target gas molecules and the resistance of sensor will changed immediately. After a while, the resistance becomes stable again, noted the value as R_g. In the end, the sensor was transferred back into the chamber 1, which was full of fresh air and the resistance of the sensor will recover. In this process, the resistance of the sensor was monitored and recorded in real time by the high precision digital multimeter, and the curve of the resistance changing continuously with time was finally displayed on the computer. The gas response of the sensor is defined as the ratio of R_a/R_g. In addition, when the sensor was exposed to the test gas, the time taken by the sensor for the change of resistance from R_a to R_a – 90% (R_a–R_g) was noted as the response time (τ_{res}). When the sensor was detached from the test gas, the time taken by the sensor for the change of resistance from R_g to R_g + 90% (R_a–R_g) was noted as the recovery time (τ_{recov}). According to the definition of response and recovery time, we could obtain the corresponding response and recovery time from the continuous curve of sensor resistance recorded by the high precision digital multimeter.

3. Results and discussion

3.1. Structural and morphological characteristics

The XRD patterns of the pure and 1, 2, 3 mol% Ru-doped SnO_2 nanofibers are shown in Fig. 3. From Fig. 3(a), we could observe that all the diffraction peaks of the four samples could be indexed to tetragonal rutile structure of SnO_2, which were agreed well with the recorded values from the Joint Committee on Powder Diffraction Standards card (JCPDS 41-1445). In addition, as shown in Fig. 3(b), we could clearly observe that the diffraction peaks shifted to high angle with increasing the Ru doping amount by comparing the peaks (110) and (101) of the four samples. It could account for the difference radius of Ru^{4+} and Sn^{4+}. The radius of Sn^{4+} was 0.690 Å, which was larger than that of Ru^{4+} (0.620 Å). When the Ru^{4+} was introduced into the SnO_2 lattice, Ru^{4+} replaced the lattice position of Sn^{4+}, causing the decrease of the interplanar spacing (d) of SnO_2. According to the Bragg's Law ($n\lambda = 2d\sin\theta$), when the interplanar spacing (d) decreased, Bragg diffraction

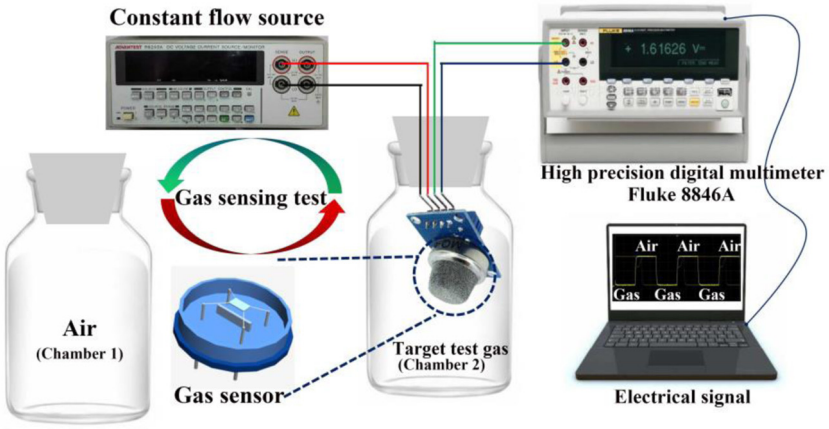

Fig. 2. Schematic diagram of static gas sensing characterization system.

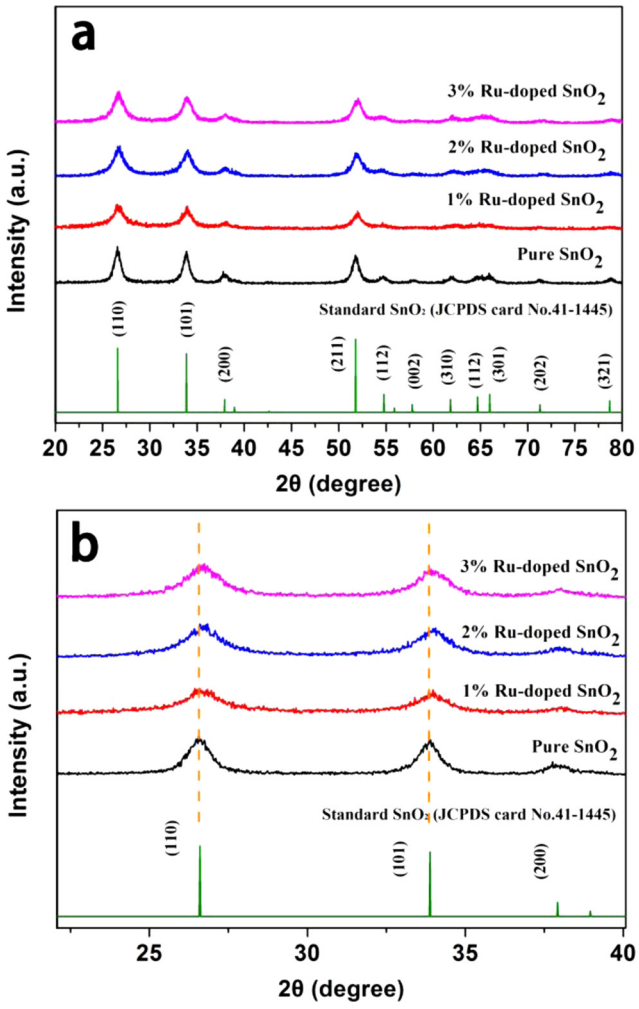

Fig. 3. (a) XRD patterns of Ru-doped SnO_2 nanofibers with different doping amount, (b) Comparison of (110) and (101) peaks from XRD patterns.

angle (θ) would increased. Therefore, the diffraction peaks shifted to high angle with Ru doping, which confirmed that Ru^{4+} was incorporated into the SnO_2 lattice, successfully. Moreover, according to the Debye-Scherrer formula,

$$D = \frac{0.89 \times \lambda}{\beta \times \cos\theta} \quad (1)$$

where λ is the X-ray wavelength (0.154056 nm), θ is the Bragg diffraction angle and β is the peak width at half maximum, using the results of the XRD characterization, we calculated the average grain size of pure, 1, 2 and 3 mol% Ru-doped SnO_2 samples as 9.18, 6.74, 6.12, and 5.05 nm, respectively, which indicated that the incorporation of Ru^{4+} could effectively prevent the grain growth of SnO_2.

FESEM images of pure and 1 − 3 mol% Ru-doped SnO_2 nanofibers were shown in Fig. 4(a)–(d). We could observe that all the samples showed fibrous nanocrystalline morphology with a uniform diameter about 120–150 nm. The samples exhibited a net structures of nanofibers, which was advantageous for the target gas to easily diffuse or overflow between the surface and the internal of sensing materials. In addition, we could observe that all the samples were composed of a lot of small nanoparticles. The insets of the figures are the enlarged details of the four samples. We could observe from the insets that the SnO_2 nanofibers became more compact and the porosity reduced with increasing the Ru doping amount. Based on the results of XRD characterization, we analyzed that the decreased porosity of SnO_2 nanofibers may be due to the reduction of the grain size of the nanoparticles which consist of the nanofibers. XRD results confirmed that with the increase of Ru doping amount, the grain size of SnO_2 gradually reduced. It is easy to understand that the smaller size of the nanoparticles consisting of the nanofibers, the more compact and smoother of the surface of the nanofibers exhibited.

TEM characterization was carried out to further explore the internal structure of pure SnO_2 and 2 mol% Ru-doped SnO_2 nanofbers, as shown in Fig. 5. Fig. 5(a) and (d) are the TEM images of pure and 2 mol% Ru-doped SnO_2 nanofibers, while Fig. 5(b) and (e) are the high-magnification TEM images of the corresponding two samples. From the images we could clearly observe that the microstructures of the two samples were similar to the FESEM results. The two samples were all of nanofibrous structure and formed a network. In addition, the sample doped with 2 mol% Ru was a little tighter than the pure one, which was as same as the FESEM results. According to the XRD results, we knew that the average grain size of pure SnO_2 was 9.18 nm, which was larger than the 2 mol% Ru doped one (6.12 nm). So, the smaller grain size resulted in the tighter of the samples. TEM results further confirmed that Ru doping changed the microstructures of SnO_2 nanofibers. The HRTEM images and SAED patterns of the two samples were shown in Fig. 5 (c) and (f), which indicated that the SnO_2 nanofibers were composed of highly crystalline nanoparticles and polycrystalline in nature. We could observe the lattice fringes clearly in the insets of Fig. 5(c) and (f) and the interplanar spacings were 0.334 nm, corresponding to the (110) planes of SnO_2, indicating the two samples are all SnO_2. Figs. 5(g)–(j) show the EDS elemental mapping images, indicating these nanofibers were comprised of Sn, O and Ru, and the Ru elements were evenly distributed among the SnO_2 nanofibers.

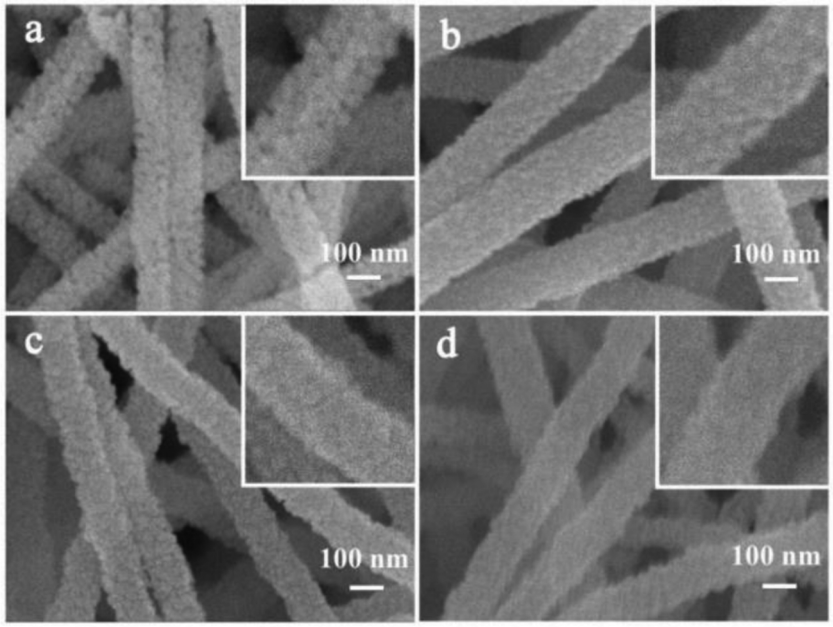

Fig. 4. FESEM images of (a) pure (b) 1 mol% (c) 2 mol% (d) 3 mol% Ru-doped SnO_2 nanofibers.

3.2. Gas sensing characteristics

First, we investigated the influence of operating temperature and doping amount on gas sensing properties of pure, 1, 2, 3 mol% Ru doped SnO_2 nanofibers. The gas responses of the sensors based on the four samples to 100 ppm acetone were tested at different operating temperatures from 167 to 239 ℃, as shown in Fig. 6. Obviously, the relation curves of response to operating temperature of all samples exhibited a volcano-shaped, and the optimal operating temperature of every sample was 200℃. In addition, we could observed that the gas response was greatly improved after Ru doping. The gas responses of the sensors based on the pure, 1, 2 and 3 mol% Ru-doped SnO_2 to 100 ppm acetone at 200 ℃ were 10.0, 33.6, 118.8, and 52.0, respectively. The results indicated that the optimal doping amount was 2 mol % according to the highest response (118.8) to 100 ppm acetone of sensors based on 2 mol% Ru-doped SnO_2, and the response value was about 12 times higher than that of pure SnO_2. The maximum response to 100 ppm acetone decreased to 52.0, while increased the Ru doping amout to 3 mol%. However, the response was still 5.2 times higher than that of the pure SnO_2 sensor.

Fig. 7(a) showed the dynamic response characteristics of sensors based on the 2 mol% Ru-doped SnO_2 nanofibers to 100 ppm acetone at 200 ℃. We could observe from the figure that the sensor exhibited a continuous and intact response-recovery curve with a short response

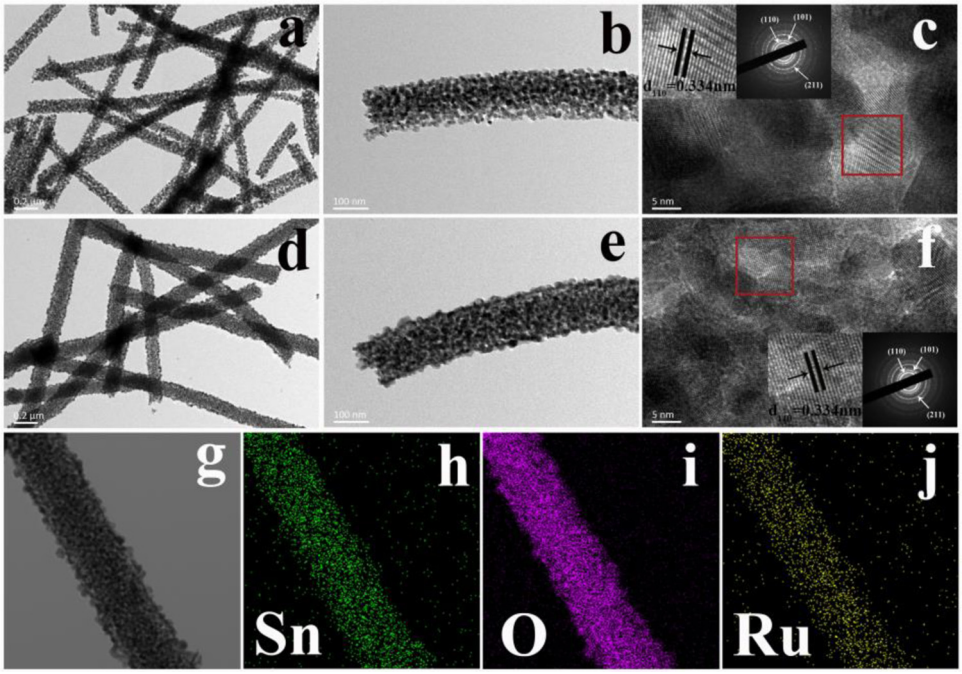

Fig. 5. TEM images of (a–c) pure SnO_2 naofibers, (d–f) 2 mol% Ru-doped SnO_2 nanofibers, and (g–j) EDS elemental mapping images of Sn, O and Ru in 2 mol% Ru-doped SnO_2 nanofibers.

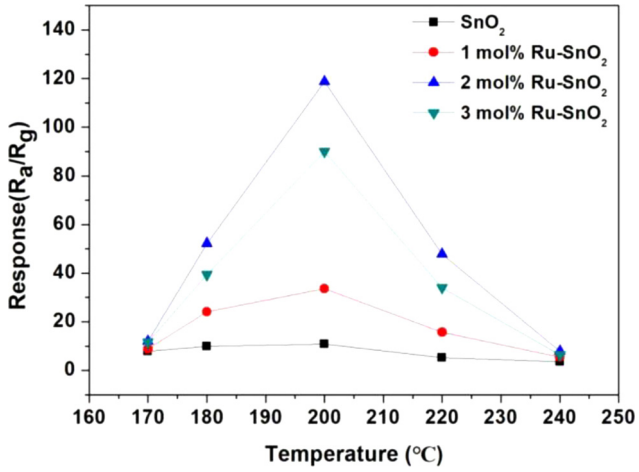

Fig. 6. Response of sensors based on pure and 1, 2, 3 mol% Ru-doped SnO_2 nanofibers to 100 ppm acetone as a function of the operating temperature.

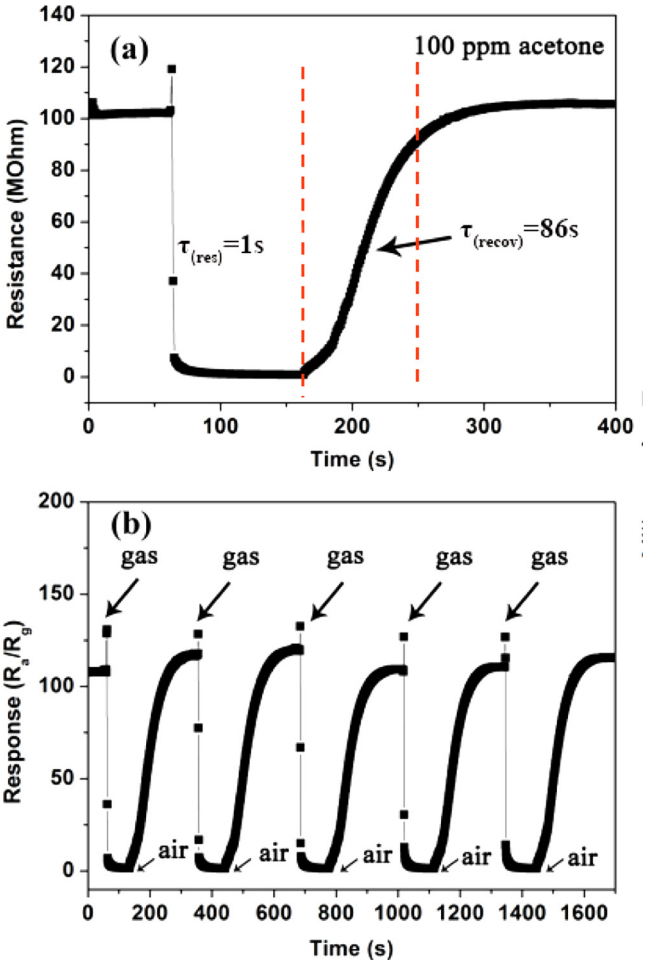

Fig. 7. (a) Response and recovery curves. (b) Five reversible cycles of sensor based on 2 mol% Ru-doped SnO_2 nanofibers to 100 ppm acetone at 200 ℃.

time of 1 s and recovery time of 86 s. Then, five reversible cycles of the response curves with little deviation were shown in Fig. 7(b), which fully illustrated that the sensor exhibited a excellent stability and repeatability.

The dynamical response-recovery curves of sensors based on pure SnO_2 and 2 mol% Ru-doped SnO_2 nanofibers toward different concentration of acetone at 200 ℃ were shown in Fig. 8(a). We could

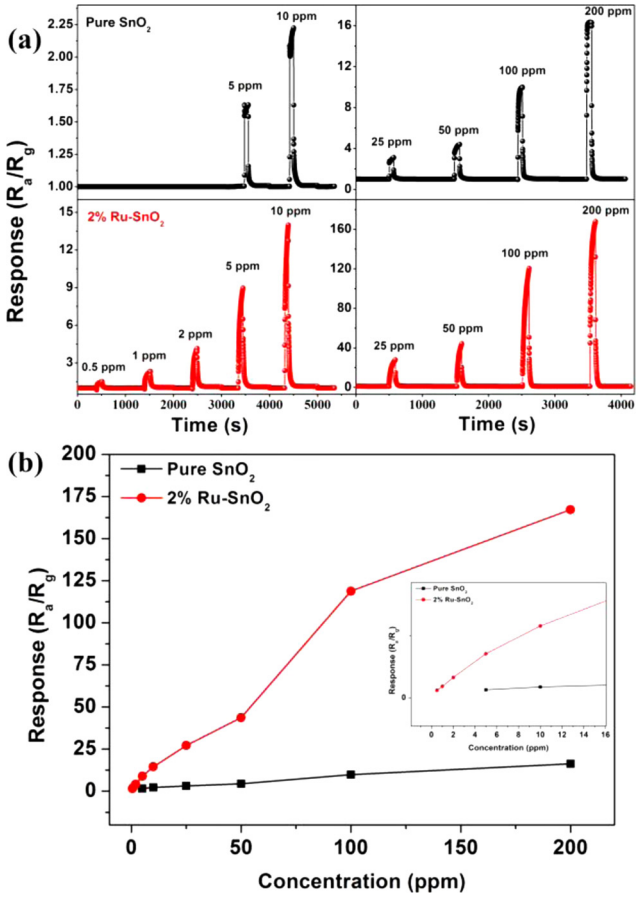

Fig. 8. (a) The dynamic response curves of sensors based on pure SnO_2 and 2 mol% Ru-doped SnO_2 nanofibers versus acetone concentration in the range of 0.5–200 ppm at 200 ℃ (b) is the corresponding linear graph of (a).

observe that the responses to acetone of the two sensors enhanced while we increased the concentrations of the acetone gas. In addition, it was obviously that the response of the sensor based on 2 mol% Ru-doped SnO_2 nanofibers was greatly higher than that of the pure SnO_2 nanofibers. Fig. 8(b) showed the corresponding linear graph of Fig. 8(a). The responses of sensor based on pure SnO_2 nanofibers were 1.6, 2.2, 3.1, 4.4, 9.9, 16.3 to 5, 10, 25, 50, 100, 200 ppm acetone, while the responses of sensor based on 2 mol% Ru-doped SnO_2 nanofibers were 8.9, 14.5, 27.1, 43.7, 118.8, 167.2 to 5, 10, 25, 50, 100, 200 ppm acetone, respectively. In addition, the minimum acetone detection limit of the sensor based on 2 mol% Ru-doped SnO_2 nanofibers was measured as 0.5 ppm, while the minimum acetone detection limit of the pure one was measured as 5 ppm. It is worth noting that the response of the sensor based on 2 mol% Ru-doped SnO_2 nanofibers did not tend to be saturated when the acetone concentrations were raised to 200 ppm, which indicated that the sensor was suitable for a wide range of acetone detection. Therefore, the results proved that the sensor based on 2 mol % Ru-doped SnO_2 nanofibers exhibited not only a good response-recovery properties, but also a wide detection range.

Subsequently, the gas responses of sensors based on pure SnO_2 and 2 mol% Ru-doped SnO_2 nanofibers to 100 ppm of seven VOCs at 200℃ were tested. The test VOCs were ethanol (C_2H_6O), acetone (C_3H_6O), methanol (CH_4O), formaldehyde (CH_2O), toluene (C_7H_8), benzene (C_6H_6) and xylene (C_8H_{10}). As shown in Fig. 9, the sensor based on 2 mol% Ru-doped SnO_2 samples exhibited enhanced response for each test gas compared with the pure SnO_2. Additionally, the response of the sensor based on 2 mol% Ru-doped nanofibers to acetone were visibly higher than other gases, having a response of 118.8–100 ppm acetone, which was 12 times higher than pure SnO_2 at 200 ℃. Meanwhile, the

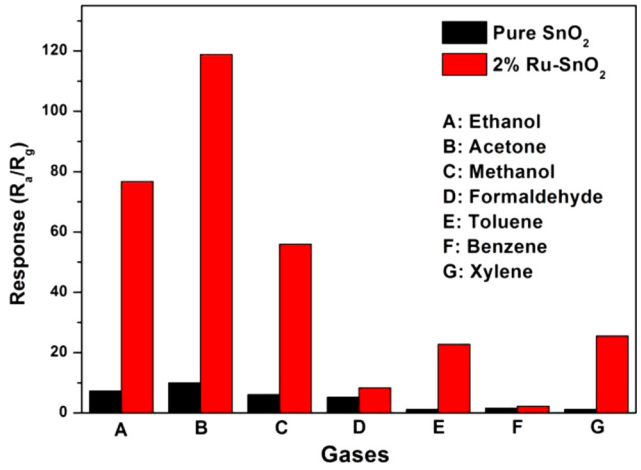

Fig. 9. Gas responses of sensors based on pure SnO_2 and 2 mol% Ru-doped SnO_2 nanofibers to 100 ppm various target gases at 200℃.

responses to 100 ppm ethanol (R_a/R_g = 76.7), methanol (R_a/R_g = 55.9), formaldehyde (R_a/R_g = 8.28), toluene (R_a/R_g = 22.8), benzene (R_a/R_g = 2.2) and xylene (R_a/R_g = 25.5) at 200 ℃ were also enhanced by Ru doping. So, It was indicated that the sensors based on Ru-doped SnO_2 nanofibers could detect acetone, selectively.

3.3. Mechanism of the enhanced gas sensing performance

In consideration of the fact that the gas sensing properties of gas sensor are greatly influenced by the carrier concentration and the chemisorbed oxygen species on the surface of the sensing materials, we investigated the electrical conductivity and the distribution of chemisorbed oxygen species of the pure and Ru-doped SnO_2 nanofibers [39]. First, we examined the electrical conductivity of pure and Ru-doped SnO_2 samples in air (R_a), the results showed that the resistances of the sensors increased after Ru doping. The resistance of sensor based on pure SnO_2 was 0.05 M Ω at 200 ℃ while the resistance of sensor based on 2 mol% Ru-doped SnO_2 was 102.2 M Ω at the same temperature. The increase of R_a after Ru doping might be due to the decrease of the grain size of SnO_2. From the results of FESEM and XRD, we knew that Ru doping could effectively inhibit the grain growth of SnO_2. It was reported that the resistance of the oxide semiconductor would increase when the grain size decrease, meanwhile resulting in an improvement of the gas sensing properties of the gas sensor [41]. In addition, Fig. 10 showed the UPS results of pure SnO_2 and 2 mol% Ru-doped SnO_2 nanofibers. The curves of the cut-off edges of the two samples were given by the results and according to the equation that $\varphi = h\mu - E_{cut\text{-}off}$, we calculated the work function (φ) of 2 mol% Ru-doped SnO_2 (21.22–16.17 eV = 5.05 eV) is smaller than that of pure SnO_2 (21.22–16.15 eV = 5.07 eV). Since the work function of oxide semiconductor nanomaterials was less than the electron affinity potential of oxygen, the oxygen molecules could grab electrons from the conduction band and increase the resistance of oxide semiconductor nanomaterials. The smaller work function of oxide semiconductor meant that more electrons could participate in the transfer, which led to further increase of the resistance [40]. Additionally, the lower electron concentration of the Ru-doped SnO_2 nanofibers could be equivalent to the larger Debye length than that of pure SnO_2 nanofibers. According to the space charge model of n-type oxide semiconductor based gas sensors, when the grain size of the sensing materials was below or equal to twice of the Debye length, the space charge layer of the grain surface completely exhausted, which could improve the gas sensing properties of the sensing materials, significantly [41].

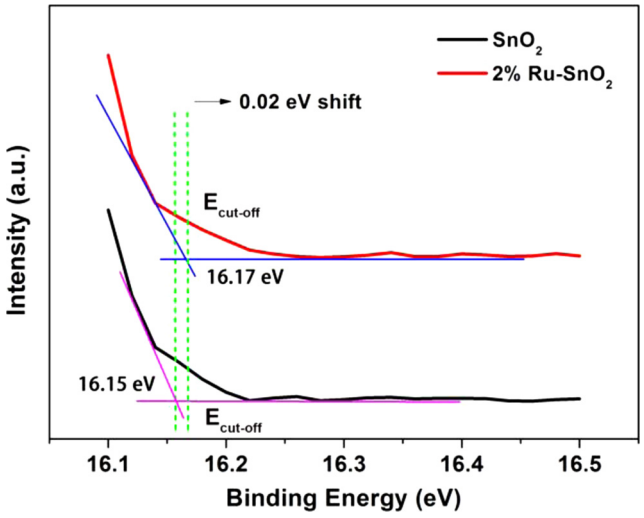

Fig. 10. UPS spectras of pure and 2 mol% Ru-doped SnO_2 nanofibers.

To further investigate the cause of the improvement in gas sensing properties of Ru-doped SnO_2 nanofibers, XPS analysis were performed. The high-resolution spectras of Sn 3d were shown in Fig. 11(a). The peaks occured at 486.58 and 495.03 eV, which were assigned to Sn $3d_{5/2}$ and Sn $3d_{3/2}$ corresponded to oxidation state +4 of tin atoms [42]. The binding energies of the Sn $3d_{5/2}$ peaks of 2 mol% Ru-doped SnO_2 samples (486.68 eV) were 0.1 eV higher than that of pure SnO_2 (486.58 eV). The peaks shift to high binding energy were caused by the loss of electrons in SnO_2 after Ru doping, confirming the incorporation of Ru into the SnO_2 lattice. Fig. 11(b) showed the spectras of Ru 3p of 2 mol% Ru-doped SnO_2 and pure SnO_2 samples. Compared with pure SnO_2, the Ru related peaks of 2 mol% Ru-doped SnO_2 was certainly detected while it was not detected in pure SnO_2. The peak of Ru $3p_{3/2}$ was occured at 463.2 eV, corresponding to oxidation state +4 of Ru atoms. In addition, Fig. 11(c)–(d) were the spectras of O 1s of pure SnO_2 and 2 mol% Ru-doped SnO_2. From the figure we could observe the O 1s peaks were asymmetric and could be decomposed into three different components, which occured at 529.5 ± 0.4 eV, 531.2 ± 0.6 eV, and 532.5 ± 0.2 eV, corresponding to lattice oxygen (O_L), oxygen vacancy (O_V), and chemisorbed oxygen species (O_C), respectively [43]. Furthermore, the percentages of O_L, O_V, and O_C components were 44.02, 21.32, and 34.66% in the pure SnO_2, while they were 14.90, 58.77, and 26.33% in the 2 mol% Ru-doped SnO_2. Obviously, the O_V and O_C were greatly increased after the incorporation of Ru element to SnO_2. At present, the widely accepted sensing mechanism of oxide semiconductor gas sensors was the change of carrier concentration caused by the oxidation reduction reactions between the chemisorbed oxygen on the surface of the sensing materials and the target gas. The increase of O_V component could provide more active sites for the oxidation reduction reactions on the surface of the sensing materials. Whereas, the increase of O_C component meant that more chemisorbed oxygen species could participate in the oxidation reduction reactions on the surface of the SnO_2 nanomaterials and thus resulted in a larger response in the gas sensing properties of sensing materials.

4. Conclusion

In summary, pure and 1–3 mol% Ru-doped SnO_2 nanofibers were synthesized through a simple electrospinning technique, combined with calcination treatment. In gas sensing applications, a systematic and comprehensive test was performed. The results indicated that the 2 mol % Ru-doped SnO_2 nanofibers showed greatly enhanced gas sensing performance, specially exhibiting a excellent sensibility to acetone gas. At last, according to the results of XPS and UPS, we analyzed the changes of the electron concentration and distribution of oxygen component caused by the incorporation of Ru^{4+} into SnO_2 nanocrystals played an important role in increase of gas sensing performance. Thus,

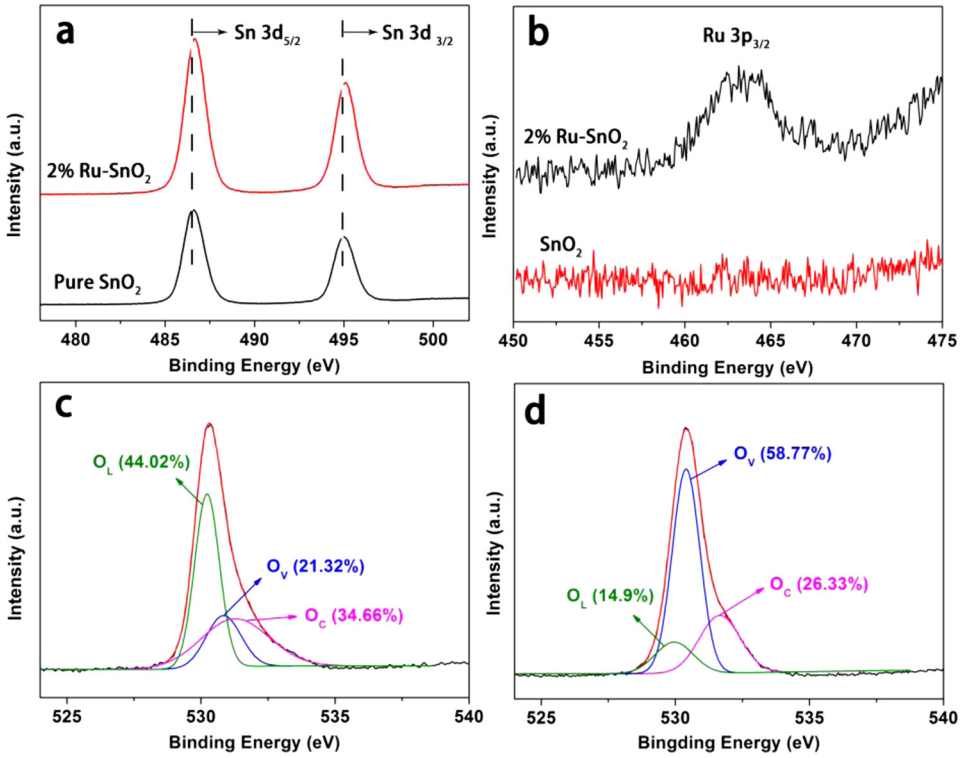

Fig. 11. XPS spectra of SnO_2 naofibers and Ru-doped SnO_2 naofibers. (a) Sn 3d for pure and 2 mol% Ru-doped SnO_2, (b) Ru 3p for Ru-doped samples, (c–d) O 1s XPS spectra of the pure and 2 mol% Ru-doped SnO_2 naofibers.

the doping of Ru^{4+} into SnO_2 nanofibers should be a promising strategy for designing and fabricating high performance acetone gas sensor.

Acknowledgements

This work was supported by National Nature Science Foundation of China (Nos. 61722305, 61833006, 61520106003, 61831011, 61803171, 61871198, and 21806051). Program for JLU Science and Technology Innovative Research Team No. JLUSTIRT 2017TD-07.

References

[1] Ananya Dey, Semiconductor metal oxide gas sensors: a review, Mater. Sci. Eng. B 229 (2018) 206–217.
[2] K. Wetchakun, T. Samerjai, N. Tamaekong, C. Liewhiran, C. Siriwong, V. Kruefu, A. Wisitsoraat, A. Tuantranont, S. Phanichphant, Semiconducting metal oxides as sensors for environmentally hazardous gases, Sens. Actuators B 160 (2011) 580–591.
[3] Jae-Hun Kim, Ali Mirzaei, Jin-Young Kim, Jae-Hyoung Lee, HyounWoo Kim, Shunich Hishita, Sang Sub Kim, Enhancement of gas sensing by implantation of Sb-ions in SnO_2 nanowires, Sens. Actuators B 304 (2020) 127307.
[4] Hee-Jin Cho, Seon-Jin Choi, Nam-Hoon Kim, Il-Doo Kim, Porosity controlled 3D SnO_2 spheres via electrostatic spray: selective acetone sensors, Sens. Actuators B 304 (2020) 127350.
[5] Fang Chen, Man Yang, Xi Wang, Yang Song, Lanlan Guo, Ning Xie, Xueying Kou, Xiumei Xu, Yanfeng Sun, Geyu Lu, Template-free synthesis of cubic-rhombohedral-In_2O_3 flower for ppb level acetone detection, Sens. Actuators B 290 (2019) 459–466.
[6] Lanlan Guo, Fang Chen, Ning Xie, Xueying Kou, Chong Wang, Yanfeng Sun, Fangmeng Liu, Xishuang Liang, Yuan Gao, Xu Yan, Tong Zhang, Geyu Lu, Ultra-sensitive sensing platform based on Pt-ZnO-In_2O_3 nanofibers for detection of acetone, Sens. Actuators B 272 (2018) 186–194.
[7] MohammedMuzibur Rahman, Efficient formaldehyde sensor development based on Cu-codoped ZnO nanomaterial by an electrochemical approach, Sens. Actuators B 305 (2020) 127541.
[8] Saisai Zhang, Yanwei Li, Guang Sun, Bo Zhang, Yan Wang, Jianliang Cao, Zhanying Zhang, Synthesis of NiO-decorated ZnO porous nanosheets with improved CH_4 sensing performance, Appl. Surf. Sci. 497 (2019) 143811.
[9] Mingjing Wang, Tianyi Hou, Zhurui Shen, Xiaodong Zhao, Huiming Ji, MOF-derived Fe_2O_3: phase control and effects of phase composition on gas sensing performance, Sens. Actuators B 292 (2019) 171–179.
[10] Bo Zhang, Guannan Liu, Ming Cheng, Yuan Gao, Lianjing Zhao, Shan Li, Fangmeng Liu, Xu Yan, Tong Zhang, Peng Sun, Geyu Lu, The preparation of reduced graphene oxide-encapsulated -Fe_2O_3 hybrid and its outstanding NO_2 gas sensing properties at room temperature, Sens. Actuators B 261 (2018) 252–263.
[11] Xi Wang, Fang Chen, Man Yang, Lanlan Guo, Ning Xie, Xueying Kou, Yang Song, Qingji Wang, Yanfeng Sun, Geyu Lu, Dispersed WO_3 nanoparticles with porous nanostructure for ultrafast toluene sensing, Sens. Actuators B 289 (2019) 195–206.
[12] Meng-Di Wang, Yan-Yang Li, Bo-Han Yao, Kaihua Zhai, Zhong-Jun Lia, Hong-Chang Yao, Synthesis of three-dimensionally ordered macro/mesoporous C-doped WO_3 materials: effect of template sizes on gas sensing properties, Sens. Actuators B 288 (2019) 656–666.
[13] Q. Gao, W. Zeng, R. Miao, Synthesis of multifarious hierarchical flower-like NiO and their gas-sensing properties, J. Mater. Sci.: Mater. Electron. 27 (2016) 9410–9416.
[14] Mario Urso, SalvatoreGianluca Leonardi, Giovanni Neri, Salvatore Petralia, Sabrina Conoci, Francesco Priolo, Salvo Mirabella, Room temperature detection and modelling of sub-ppm NO_2 by low-cost nanoporous NiO film, Sens. Actuators B 305 (2020) 127481.
[15] Linxia Fang, Zongwen Zhang, Xiang Li, Hui Zhou, Keke Ma, Ling Ge, Kejing Huang, Fabrication of hybrid cauliflower-like nanoarchitectures by in situ grown ZnO nanoparticals on VS_2 ultrathin nanosheets for high performance supercapacitors, Colloid Surf. A: Physicochem. Eng. Asp. 501 (2016) 42–48.
[16] Meiling Wang, Guowen Menga, Qing Huang, Yilin Lu, Yao Gu, Fluorophore-modified Fe_3O_4-magnetic-nanoparticles for determination of heavy metal ions in water, Sens. Actuators B 185 (2013) 47–52.
[17] Hongtao Wang, Linsheng Zhou, Yueying Liu, Fengmin Liu, Xishuang Liang, Fangmeng Liu, Yuan Gao, Xu Yan, Geyu Lu, UV-activated ultrasensitive and fast reversible ppb NO_2 sensing based on ZnO nanorod modified by constructing interfacial electric field with In_2O_3 nanoparticles, Sens. Actuators B 305 (2020) 127498.
[18] Jing Wang, Saiying Fan, Yi Xia, Cheng Yang, Sridhar Komarneni, Room-temperature gas sensors based on ZnO nanorod/Au hybrids: Visiblelight-modulated dual selectivity to NO_2 and NH_3, J. Hazard. Mater. 381 (2020) 120919.
[19] Jing Wang, Mingying Yu, Yi Xia, Xian Li, Cheng Yang, Sridhar Komarneni, On-chip grown ZnO nanosheet-array with interconnected nanojunction interfaces for enhanced optoelectronic NO_2 gas sensing at room temperature, J. Colloid Interface Sci. 554 (2019) 19–28.
[20] Mingsong Wang, Qiang Luo, Shahid Hussain, Guiwu Liu, Guanjun Qiao, Eui Jung Kim, Sharply-precipitated spherical assembly of ZnO nanosheets for low temperature H_2S gas sensing performances, Mater. Sci. Semicond. Process. 100 (2019) 283–289.
[21] Kuan-Wei Chen, Ju-Heng Tsai, Chun-Hua Chen, Controlled synthesis and CO sensing potentials of size-tunable highly-uniform mesoporous Co_3O_4 nanospheres, J. Alloys Compd. 816 (2020) 152524.
[22] Ming Cheng, Zepei Wu, Guannan Liu, Lianjing Zhao, Yuan Gao, Shan Li, Bo Zhang, Xu Yan, Geyu Lu, Carbon dots decorated hierarchical litchi-like In_2O_3 nanospheres for highly sensitive and selective NO_2 detection, Sens. Actuators B 304 (2020) 127272.

[23] Dongzhi Zhang, Zhimin Yang, Peng Li, Maosong Pang, Qingzhong Xue, Flexible self-powered high-performance ammonia sensor based on Audecorated $MoSe_2$ nanoflowers driven by single layer MoS_2-flake piezoelectric nanogenerator, Nano Energy 65 (2019) 103974.
[24] Dongping Xue, Zhanying Zhang, Yan Wang, Enhanced methane sensing performance of SnO_2 nanoflowers based sensors decorated with Au nanoparticles, Mater. Chem. Phys. 237 (2019) 121864.
[25] Xueying Kou, Chong Wang, Mengdi Ding, Changhao Feng, Xin Li, Jian Ma, Hong Zhang, Yanfeng Sun, Geyu Lu, Synthesis of Co-doped SnO_2 nanofibers and their enhanced gas-sensing properties, Sens. Actuators B 236 (2016) 425–432.
[26] Jing Cao, Ningrui Zhang, Shuangming Wang, Cong Chen, Haiming Zhang, Researching the crystal phase effect on gas sensing performance in In_2O_3 nanofibers, Sens. Actuators B 305 (2020) 127475.
[27] Rongjun Zhao, Xu Zhang, Sijia Peng, Ping Hong, Tong Zou, Zidong Wang, Xinxin Xing, Yue Yang, Yude Wang, Shaddock peels as bio-templates synthesis of Cd-doped SnO_2 nanofibers: a high performance formaldehyde sensing material, J. Alloys Compd. 813 (2020) 152170.
[28] Chul-Soon Lee, Hua-Yao Li, Bo-Young Kim, Young-Moo Jo, Hyung-Gi Byun, In-Sung Hwang, Faissal Abdel-Hady, AbdulazizA. Wazzan, Jong-Heun Lee, Discriminative detection of indoor volatile organic compounds using a sensor array based on pure and Fe-doped In_2O_3 nanofifibers, Sens. Actuators B 285 (2019) 193–200.
[29] Hui Li, Shushu Chu, Qian Ma, Hang Li, Quande Che, Junpeng Wang, Gang Wang, Ping Yang, Multilevel effective heterojunctions based on SnO_2/ZnO 1D fibrous hierarchical structure with unique interface electronic effects, ACS Appl. Mater. Interfaces 11 (2019) 31551–31561.
[30] Jae-Hun Kim, Jae-Hyoung Lee, Jin-Young Kim, Ali Mirzaei, Hyoun Woo Kim, Sang Sub Kim, Enhancement of CO and NO_2 sensing in n-SnO_2-p-Cu_2O core-shell nanofibers by shell optimization, J. Hazard. Mater. 376 (2019) 68–82.
[31] Xinwei Chen, Shuai Wang, Chen Su, Yutong Han, Cheng Zou, Min Zeng, Nantao Hu, Yanjie Su, Zhihua Zhou, Zhi Yang, Two-dimensional Cd-doped porous Co_3O_4 nanosheets for enhanced roomtemperature NO_2 sensing performance, Sens. Actuators B 305 (2020) 127393.
[32] Zhi-Hong Ma, Rui-Tao Yu, Ji-Ming Song, Facile synthesis of Pr-doped In_2O_3 nanoparticles and their high gas sensing performance for ethanol, Sens. Actuators B 305 (2020) 127377.
[33] Bumhee Nam, Tae-Kyoung Ko, Soong-Keun Hyun, Chongmu Lee, Sensitivities of a 6:4 (by molar ratio) ZnO/WO_3 composite nanoparticle sensor to reducing and oxidizing gases, Appl. Surf. Sci. 504 (2020) 144104.
[34] Zakie Anajafi, Mahmoud Naseri, G. Neri, Acetone sensing behavior of p-$SmFeO_3$/n-ZnO nanocomposite synthesized by thermal treatment method, Sens. Actuators B 304 (2020) 127252.
[35] Chun-Han Wu, Zhen Zhu, Hong-Ming Chang, Zong-Xian Jiang, Chia-Ying Hsieh, Ren-Jang Wu, Pt@NiO core–shell nanostructure for a hydrogen gas sensor, J. Alloys Compd. 814 (2020) 151815.
[36] Yan Wang, Xiao-ning Meng, Jian-liang Cao, Rapid detection of low concentration CO using Pt-loaded ZnO nanosheets, J. Hazard. Mater. 381 (2020) 120944.
[37] Chen Wang, Xiaobiao Cui, Jiangyang Liu, Xin Zhou, Xiaoyang Cheng, Peng Sun, Xiaolong Hu, Xiaowei Li, Jie Zheng, Geyu Lu, Design of superior ethanol gas sensor based on Al-doped NiO nanorod-flowers, ACS Sens. 1 (2016) 131–136.
[38] Xueying Kou, Ning Xie, Fang Chen, Tianshuang Wang, Lanlan Guo, Chong Wang, Qingji Wang, Jian Ma, Yanfeng Sun, Hong Zhang, Geyu Lu, Superior acetone gas sensor based on electrospun SnO_2 nanofifibers by Rh doping, Sens. Actuators B 256 (2018) 861–869.
[39] Chen Wang, Jiangyang Liu, Qiuyue Yang, Peng Sun, Yuan Gao, Fengmin Liu, Jie Zheng, Geyu Lu, Ultrasensitive and low detection limit of acetone gas sensor based on W-doped NiO hierarchical nanostructure, Sens. Actuators B 220 (2015) 59–67.
[40] Tianshuang Wang, Bin Jiang, Qi Yu, Xueying Kou, Peng Sun, Fangmeng Liu, Huiying Lu, Xu Yan, Geyu Lu, Realizing the control of electronic energy level structure and gas sensing selectivity over heteroatom-doped In_2O_3 spheres with an inverse opal microstructure, Appl. Mater. Interfaces 11 (2019) 9600–9611.
[41] N. Yamazoe, G. Sakai, K. Shimanoe, Oxide semicomductor gas sensors, Catal. Surv. Asia 7 (2003) 63–75.
[42] Jun Zhang, Xianghong Liu, Shihua Wu, Mijuan Xu, Xianzhi Guo, Shurong Wang, Au nanoparticle-decorated porous SnO_2 hollow spheres: a new model for a chemical sensor, J. Mater. Chem. 20 (2010) 6453–6459.
[43] Mohammad R. Alenezi, Abdullah S. Alshammari, K.D.G.I. Jayawardena, Michail J. Beliatis, Simon J. Henley, S.R.P. Silva, Role of the exposed polar facets in the performance of thermally and UV activated ZnO nanostructured gas sensors, J. Phys. Chem. C 117 (2013) 17850–17858.

Xueying Kou received the B. Eng. degree in department of electronic sciences and technology in 2015. She is currently studying for her PhD degree in College of Electronic Science and Engineering, Jilin University, China. Now, she is engaged in the synthesis and characterization of the semiconducting functional materials and gas sensors.

Fanqi Meng received the B. Eng. degree in Department of Electronic Science and Engineering in 2019. She is currently studying for her MS degree in College of Electronic Science and Engineering, Jilin University, China.

Ke Chen received the BS degree in Department of Electronic Science and Engineering in 2019. She is currently studying for her MS degree in College of Electronic Science and Engineering, Jilin University, China.

Tianshuang Wang received his B. Eng. degree from the Electronics Science and Engineering department, Jilin University, China in 2015. Presently, he is studying for his PhD degree in College of Electronic Science and Engineering, Jilin University, and interesting in the synthesis and characterization of the semiconducting functional materials and gas sensors.

Peng Sun received his PhD degree from College of Electronic Science and Engineering, Jilin University, China in 2014.Now he is a professor of Jilin University. He is engaged in the gas sensors based on oxide semiconductors.

Fangmeng Liu received his PhD degree in 2017 from College of Electronic Science and Engineering, Jilin University, China. Now he is a lecturer of Jilin University, China. His current research interests include the application of functional materials and development of solid state electrochemical gas sensor and flexible device.

Xu Yan received his M.S. degree in 2013 from Nanjing Agricultural University. He joined the group of Prof. Xingguang Su at Jilin University and received his PhD degree in June 2017. Since then, he did postdoctoral work with Prof. Geyu Lu. Currently, his research interests mainly focus on the development of the functional nanomaterials for chem/bio sensors.

Yanfeng Sun obtained his PhD from Jilin University of China in 2007. Presently, he is working as a professor in Electronics Science and Engineering department of Jilin University. His current research interests are nanoscience and gas sensors.

Fengmin Liu received the BE degree in Department of Electronic Science and Technology in 2000. She received her Doctor's degree in College of Electronic Science and Engineering at Jilin University in 2005. Now she is a professor in Jilin University, China. Her current research is preparation and application of semiconductor oxide, especial in gas sensor and solar cell.

Kengo Shimanoe has been a professor at Kyushu University since 2005. He received a B. Eng. degree in applied chemistry in 1983 and a M. Eng. degree in 1985 from Kagoshima University and Kyushu University, respectively. He joined Nippon Steel Corp. in 1985, and received a Dr. Eng. degree in 1993 from Kyushu University. His current research interests include the development of gas sensors and other functional devices.

Geyu Lu received the BS degree in electronic sciences in 1985 and the MS degree in 1988 from Jilin University in China and the Dr. Eng. degree in 1998 from Kyushu University in Japan. Now he is a professor of Jilin University, China. His current research interests include the development of chemical sensors and the application of the function materials.